

Elimination of CO₂/N₂ Langmuir Sorption and Promotion of “N₂-phobicity” within High T_g, Glassy Membranes

Christopher R. Maroon,[†] Jacob Townsend,[†] Kevin R. Gmernicki,[†] Daniel J. Harrigan,[‡] Benjamin J. Sundell,[‡] John A. Lawrence III,[‡] Shannon M. Mahurin,[§] Konstantinos D. Vogiatzis,[†] Brian K. Long^{†*}

[†]Department of Chemistry, University of Tennessee, Knoxville, Tennessee, 37996-1600

[‡]Aramco Services Company: Aramco Research Center - Boston, Massachusetts, 02139

[§]Chemical Sciences Division, Oak Ridge National Laboratory, Oak Ridge, Tennessee 37831

KEYWORDS: Vinyl-addition polymerization, norbornene, neutral Ni catalyst, ethylene glycol, amorphous, CO₂/N₂ membrane

ABSTRACT: Herein, we demonstrate that the CO₂/N₂ gas separation performance of alkoxy-silyl-substituted vinyl-added polynorbornenes (VAPNBs) may be significantly enhanced via incorporation of the monomer, 5-tris(2-methoxyethoxy)silyl-2-norbornene. As the molar ratio of this monomer is increased, substantial increases in CO₂/N₂ selectivity are realized with minimal decrease in CO₂ permeability. This trend ignores the traditional permeability/selectivity “tradeoff” relationship, and yields an optimal membrane whose performance reaches the 2008 Upper Bound for CO₂/N₂ separations. Though the inclusion of 5-tris(2-methoxyethoxy)-silyl-2-norbornene units was initially hypothesized to maximize CO₂ solubility, detailed gas sorption studies reveal that these highly glassy materials essentially lack any Langmuir sorption component, and indicate that their improved CO₂/N₂ selectivity is due to decreased N₂ solubility within the matrix. Computational modelling suggests that the source of this apparent “N₂-phobicity” is likely explained through comparative analyses of polymer-polymer and polymer-gas interactions. Lastly, mixed-gas permeation tests are performed to provide a more realistic look at real-world gas separation performance.

1. Introduction

The implementation of successful methods for carbon capture and sequestration (CCS) is vital to controlling the emission of greenhouse gases such as carbon dioxide (CO₂). These emissions have been linked to increasing global temperatures, rising sea levels, varying weather patterns, and changes to ecosystems and habitats.¹ A major contributor to these emissions are coal and gas-fired power plants that are necessary for sustaining the population’s current and future energy demands. In particular, coal combustion is believed to be responsible for approximately one-third of all current U.S. based carbon dioxide emissions, and studies have projected that the use of coal will continue to increase until the year 2050.^{2,3} To remedy this, steps toward effective CO₂ capture are necessary.^{4,5,6}

Amongst the various CO₂ capture methods being pursued, polymeric membranes present several advantages including a more passive separation mechanism, lower operating costs, and a smaller environmental footprint than rivaling amine absorption

systems. However, if polymer membranes are to reach suitable performance targets for CCS, further advancements in membrane performance must be realized.^{4,7} Unfortunately, this pursuit is frequently hindered by the inherent tradeoff relationship in which more selective polymers are generally less permeable, whereas more permeable polymers tend to be less selective. This behavior is most easily visualized on a log-log plot of pure gas permeability versus selectivity, called a Robeson Plot, wherein an upper-bound of membrane performance has been defined.⁸⁻⁹

For most gas pairs, the highest performing membranes comprising the upper bound are glassy polymers whose selectivity values were traditionally thought to be determined primarily via diffusivity; however, more recent reports have shown that solubility also plays a key role.^{8,10-13} Because CO₂ and N₂ are known to have similar kinetic diameters (CO₂ = 3.30 Å and N₂ = 3.64 Å), enhancing polymer CO₂ selectivity via diffusivity control has proven quite challenging.¹⁴ As a result, enhancing CO₂ solubility is often hypothesized to be the most promising pathway toward meaningful advances in membrane performance. Though simple in theory, chemical modifications to enhance polymeric CO₂ solubility often succumb to the aforementioned permeability-selectivity tradeoff, which highlights the need to simultaneously maintain high permeability.

Recent efforts to address this issue have resulted in a plethora of reports in which new and/or modified polymer membranes have been examined for the separation of CO₂ and N₂ gases. Polymers that have shown notable performance include polymers of intrinsic microporosity (PIMs),¹⁵⁻²³ polyacetylenes,²⁴⁻²⁸ modified polydimethylsiloxanes,²⁹⁻³⁰ poly(ethylene oxide),³¹⁻³⁵ and functionalized vinyl-added polynorbornenes (VAPNBs).³⁶⁻⁴¹ Amidst these high performing polymers, noteworthy features include either rigid polymer backbones, which frustrate inter-chain packing, and/or Lewis basic functionalities that are hypothesized to form favorable interactions with gasses such as CO₂.^{37,42-44}

To combine the advantages of both polymer backbone rigidity and Lewis basic functionality, Sundell *et al.* and Long *et al.* each recently developed a class of alkoxy-silyl-substituted VAPNBs for gas separation applications.^{41,45-47} Prior to these reports, such materials were only obtained as low molecular weight oligomers, and thus not suitable for membrane formation. However, through careful catalyst selection, both groups demonstrated that alkoxy-silane-substituted VAPNBs could be synthesized in acceptable yields (> 65 %) and high molecular weights ($M_n > 120$ kg/mol). Thermal analyses revealed that these polymers are glassy materials with glass transition (T_g) and decomposition (T_d) temperatures exceeding 300 °C.⁴⁶ Detailed investigations revealed that gas selectivity in these alkoxy-silyl-substituted VAPNBs is primarily dominated by solubility control, making them attractive targets for gas separations such as CO₂/N₂, C₃H₈/CH₄, and C₄H₁₀/CH₄, which contain condensable gas components.

Having established that this class of alkoxy-silyl-substituted VAPNBs are glassy polymers whose transport is primarily governed via solubility control,⁴⁶ we hypothesized that their gas separation performance may be enhanced via the incorporation of more CO₂-philic functionalities. Though numerous moieties are known to have favorable interactions with CO₂,⁴⁸⁻⁴⁹ we were particularly interested in those containing ethylene glycol-like fragments. Such moieties are commonly found in poly(ethylene oxide) (PEO)³¹ and its related copolymers,⁵⁰⁻⁵¹ which often demonstrate high CO₂/N₂ selectivities. Therefore, in an effort to enhance the CO₂

solubility and overall gas separation performance of alkoxy silane-substituted VAPNBs, we herein describe the synthesis and systematic evaluation of polymers **P1-P5** (Figure 1).

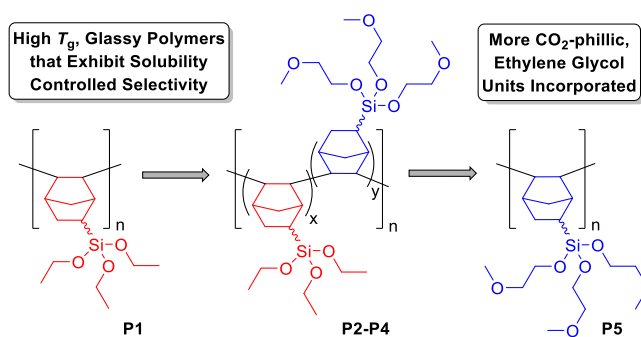


Figure 1. Polymers **P1-P5** containing 5-triethoxysilyl-2-norbornene (red) and 5-tris(2-methoxyethoxy)-2-norbornene (blue) units.

Polymers **P1-P5** systematically introduce CO₂-philic, ethylene glycol-like moieties via the (co)polymerization of norbornyl monomers bearing tris-(2-methoxyethoxy)silane substituents (shown in blue in Figure 1). Therein, polymer **P1** contains no monomers with ethylene glycol-like units, copolymers **P2-P4** are comprised of increasing percentages of monomers with ethylene glycol-like units, and finally polymer **P5** contains 100 mol% monomers bearing ethylene glycol-like moieties. The detailed evaluation of these polymers presented herein will demonstrate that as the mole fraction of repeat units containing these tris-(2-methoxyethoxy)silane units increases, their gas separation performance is enhanced significantly, virtually reaching the 2008 “Upper Bound”.⁸ Interestingly, this behavior overcomes the traditional permeability selectivity tradeoff relationship. Insight into the source of this intriguing behavior is provided through determination of individual diffusivity and solubility constants, sorption isotherm analysis, computational support, and mixed-gas permeation behavior.

2. Experimental Section

2.1. General Materials and Methods. All air-free reactions were conducted under an inert atmosphere using an MBraun glovebox and a dry nitrogen atmosphere. Once synthesized, monomers were degassed via freeze-pump-thaw (x3) and stored over 3 Å molecular sieves in the glovebox prior to use. Dicyclopentadiene, hydroquinone, and n-butyllithium (1.6 M in hexanes) were purchased from Acros Organics and used as received. Dichloromethane, diethyl ether, and tetrahydrofuran were purchased from Fisher Scientific and purified by passage through an Innovative Technologies PureSolv Solvent Purification System and degassed via freeze-pump-thaw (x3) prior to use. Methanol for polymer precipitation and tetrahydrofuran for film casting were used as received from Fisher Scientific. Alkoxyvinylsilane reagents were purchased from Gelest Inc. and used as received. The catalysts, *trans*-[Ni(C₆F₅)₂(SbPh₃)₂] and (η³-allyl)Pd(*i*-Pr₃P)Cl, were synthesized according to literature⁵²⁻⁵⁴ and stored in the glovebox prior to use. LiBARf was obtained as a gift from Boulder Scientific and used as received. The monomers 5-trimethylsilyl-2-norbornene (**C**) and 5-triethoxysilyl-2-norbornene (**A**) were prepared as previously reported.^{41,55}

2.2. Characterization. ^1H NMR spectroscopy of monomers and polymers were obtained in CDCl_3 using a Varian 500 MHz NMR and referenced to the residual solvent peak at $\delta = 7.26$ ppm. High resolution mass spectrometry was performed by using a JEOL AccuTOF equipped with a DART source. Polymers were characterized using a Tosoh EcoSEC GPC using THF at 40°C , and molecular weights were calculated relative to polystyrene standards. Thermal gravimetric analysis was performed using a TA Instruments Q50 with a ramp rate of $20^\circ\text{C}/\text{minute}$ under a N_2 purge. Glass transition temperatures were determined by dynamic mechanical analysis (DMA) using a TA Instruments RSA G2 instrument according to the procedure described in Sundell *et al.*⁴² Briefly, film samples of a uniform 5 mm width were mounted in a tension fixture. Samples were ramped at $3^\circ\text{C}/\text{min}$ and the axial force oscillated at 0.5% strain rate and 1 Hz until membrane failure was observed. The T_g was taken as the maximum of the $\text{Tan } \delta$ curve. Polymer densities were determined using a Mettler Toledo balance equipped with a density kit based upon Archimedes Principle. Wide-angle XRD measurements were performed using an Empyrean X-Ray Diffractometer from PANalytical that was equipped with a $\text{Cu K}\alpha$ source run at 45 kV and 40 mA filtered with a nickel filter.

2.3. Membrane Preparation. Membranes of polymers **P1-P5** were solution cast from solutions ranging from 4.7-6.3 wt. % in THF. As an example, 0.468 g of polymer was added to 10 mL of THF and stirred until fully dissolved. The resultant solution was taken up by syringe and filtered through a $0.45\ \mu\text{m}$ PTFE syringe filter onto either a clean glass or PTFE dish, both approximately 6 cm in diameter. Polymer P6 was cast using an identical procedure except using chloroform as the solvent. Glass casting dishes were used for polymers **P1-P2** and polymer **P6**, whereas PTFE casting dishes were used for polymers **P3-P5** due to the adhesive properties of those membranes to glass substrates. All casting solutions were covered with aluminum foil to slow evaporation, and the polymer films were removed from the substrate after slowly evaporating for 48 h. Each film was then dried *in vacuo* to constant weight before analysis.

2.4. Membrane Analysis. Polymer densities used to calculate fraction free volumes (FFVs) using the Bondi method (Eq. 1-2).

$$FFV = \frac{V - V_0}{V} \quad (1)$$

$$V_0 = 1.3V_w \quad (2)$$

Polymer d spacing was calculated using wide-angle X-ray scattering to provide the Bragg's distance (d_B) (Eq. 3) and interchain distance (d_{ic}) which uses a correction factor as described in the literature⁵⁶⁻⁵⁷ (Eq. 4).

$$d_B = \frac{\lambda}{2 \sin(\theta)} \quad (3)$$

$$d_{ic} = 1.22d_B \quad (4)$$

2.5. Permeation Analysis. Permeability measurements were made using a custom-built, constant-volume variable-pressure permeation instrument. Permeability is calculated as described by Eq. 5.⁵⁸ Downstream volumes (V_d) were calculated by sequential Burnett expansions using He gas. Thickness (l) of polymer films were measured using a micrometer and typically ranged between 120-200 μm . Upstream pressure (P_u) was recorded as an average for the duration of the steady-state permeation measurement.

Surface area of the polymer materials were measured using ImageJ software. $R = 0.278 \text{ [cm}\cdot\text{Hg}\cdot\text{cm}^3\text{]/[cm}^3\text{(STP)}\cdot\text{K]}$. Temperature was recorded as an average outside the sample cell during the course of steady-state permeation. Ideal selectivity was calculated as a ratio of $P(\text{CO}_2)/P(\text{N}_2)$.

$$P = \frac{V_d l}{P_u \text{ART}} \left[\left(\frac{dp}{dt} \right)_{ss} - \left(\frac{dp}{dt} \right)_{\text{leak}} \right] \quad (5)$$

Mixed gas permeation was performed by flowing a gas mixture containing 15% CO_2 , 85% N_2 through the permeation instrument. A retentate stream was added and the flow was metered to maintain less than 1% stage-cut (i.e. retentate flow was greater than 100 times faster than permeation rate). The permeate composition was sampled using a Shimadzu GC 2014 and the mixed gas permeability was calculated according to Eq. 6, where x_d and x_u are mole fractions of the specified gas in the upstream and downstream, respectively. Upstream fugacity (f_u) was calculated using the Peng-Robinson equation of state, and used instead of upstream pressure to account for gas phase non-idealities at elevated pressures. Mixed gas selectivity was calculated as the ratio of permeabilities

$$P = \left(\frac{x_d}{x_u} \right) \frac{V_d l}{f_u \text{ART}} \left[\left(\frac{dp}{dt} \right)_{ss} - \left(\frac{dp}{dt} \right)_{\text{leak}} \right] \quad (6)$$

2.6. Determination of Diffusivity and Solubility Coefficients. A membrane's permeability is the product of its diffusivity and solubility coefficients, as is described in Eq. 7. To determine individual diffusivity and solubility coefficients, sorption isotherms were measured for each membrane using a dual-volume dual-transducer pressure decay instrument. Concentrations were calculated as described by Koros,⁵⁹ and fitting parameters were obtained using a nonlinear regression fit of the obtained sorption isotherm following Eq. 8. Uncertainty of sorption isotherm measurements was estimated by propagation of error as outlined by Bevington.⁶⁰ Solubility coefficients were then calculated using these parameters as pressure $\rightarrow 0$ atm. With both P and S measured directly, diffusivity constants were determined algebraically using Eq. 7.

$$P = D \times S \quad (7)$$

$$S = \frac{C}{p} = k_d + \frac{C'_d b}{1 + b p} \quad (8)$$

2.7. Synthesis of 5-tris(2-methoxyethoxy)-2-norbornene (2). To a 50 mL glass pressure tube equipped with stir bar was added vinyltris(2-methoxyethoxy)silane (20.00 g, 71.33 mmol), dicyclopentadiene (4.49 g, 33.97 mmol), and hydroquinone (0.010 g, catalytic). The pressure tube was sealed and heated to 180 °C for 12 h. After cooling, the mixture was purified by successive distillations at reduced pressure (0.3 torr, 132-138 °C) to yield 3.63 g of the desired monomer (30.9 % yield) as a mixture of endo:exo isomers (endo:exo = 62:38). ¹H NMR (CDCl_3 , 293 K, endo isomer): δ (ppm) = 6.06 (1H, m), 5.87 (1H, m), 3.88 (6H, t), 3.46 (6H, t), 3.33 (12H, s), 2.89 (1H, s), 2.87 (1H, s), 1.75 (1H, m), 1.33-1.02 (3H, m), 0.48 (1H, ddd) ¹³C NMR (CDCl_3 , 293 K, endo/exo mixture):

δ (ppm) = 137.65, 135.36, 134.65, 133.73, 73.70, 73.68, 62.13, 61.89, 58.87, 58.85, 50.70, 46.96, 44.12, 42.71, 42.43, 42.12, 26.87, 26.17, 20.59, 20.05 HRMS^{calc} C₁₆H₃₀O₆Si (H⁺ adduct) = 347.1890 m/z HRMS^{expt} C₁₆H₃₀O₆Si (H⁺ adduct) = 347.1889 m/z.

2.8. Synthesis of Polynorbornenes P1-P5. All polymerizations for polymers **P1-P5** were ran under air free conditions in an MBraun glovebox using *trans*-[Ni(C₆F₅)₂(SbPh₃)₂] as the vinyl-addition catalyst and dry/degassed DCM as the solvent. In a typical polymerization, the catalyst *trans*-[Ni(C₆F₅)₂(SbPh₃)₂] (5 μ mol) was added to 5 mmol of total monomer in DCM (2 mL). The polymerizations were stirred for 24 hours before being diluted with additional DCM (10 mL) and precipitated into 250 mL of non-solvent. The non-solvents used included either methanol, acetonitrile, or hexanes depending on the feed ratio of the monomers used. Methanol was used for polymers **P1-P2**, acetonitrile cooled to -78 °C was used for polymer **P3**, and hexanes was used for polymers **P4-P5**. The precipitated polymers were isolated by vacuum filtration and dried *in-vacuo* to constant weight.

2.9. Synthesis of Poly(trimethylsilylnorbornene) (P6). Under air free conditions in an MBraun glovebox, the catalyst (η^3 -allyl)Pd(*i*-Pr₃P)Cl (5 μ mol), activator LiBARF (5 μ mol), and toluene (0.5 mL) were combined and stirred for 20 minutes. In a separate vial, monomer **C** (5 mmol) was dissolved in toluene (1.5 mL), and the resultant solution was added to the now activated catalyst solution. The polymerization was stirred for 24 hours then diluted with additional toluene (10 mL) and precipitated into 250 mL of methanol. The resultant polymer **P6** was isolated by filtration, then redissolved and stirred with activated carbon before being filtered through a neutral alumina plug. The filtrate containing polymer **P6** was then re-precipitated into methanol, isolated by vacuum filtration, and dried *in-vacuo* to constant weight.

2.10. Computational Details. Quantum chemical calculations were performed to elucidate the atomistic effects between individual repeat units of polymers **P1**, **P5**, and **P6**, and the respective gases (CO₂ and N₂). To evaluate the strength and behavior of the interactions, monomer-monomer and monomer-gas interactions were calculated using density functional theory (DFT). Due to the high flexibility of the side chains of monomers **A** and **B**, many competitive conformations were considered since conventional DFT geometry optimizations may converge to local minima on the potential energy surface (PES). Therefore, molecular dynamics (MD) simulations were performed to scan the conformational space, providing sufficiently stable starting conformations which were further optimized with DFT.

Initial structures were generated with the OPLS-AA force field⁶¹ in a periodic box at 200K in the NVT ensemble with a Nose-Hoover thermostat using a 1.0 ps time-constant and a 1.0 fs time-step. LigParGen⁶² was used for the generation of the force-field input, and all simulations were performed with the LAMMPS⁶³ software package. 10,000 time-steps were evaluated followed by a geometry optimization with respect to the force field to produce initial structures for DFT (Figure 2). Thirty conformations were considered for every monomer, monomer-CO₂, monomer-N₂, and monomer-monomer structures.

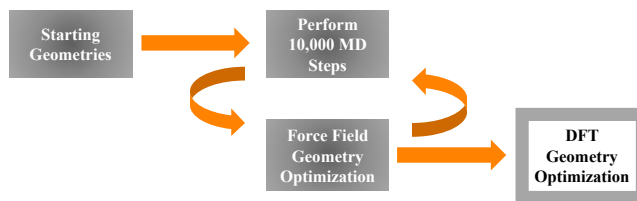


Figure 2. Flowchart of the automated conformational space search.

All DFT calculations were performed using the TURBOMOLE⁶⁴ 7.2 program package with the PBE0⁶⁵ functional, def2-TZVPP⁶⁶ basis set and Grimme’s “D3” dispersion correction⁶⁷ with the Becke-Johnson damping function.⁶⁸ An ultrafine grid was used for integral evaluation and geometry optimizations were performed with tight convergence criteria. The resolution-of-identity was used in the computation of two electron integrals. Frequency calculations were performed on the most stable conformations to ensure they are minima on the PES. Interaction energies (ΔE_{AB}) between two structures *A* and *B* were calculated using Eq. 9:

$$\Delta E_{AB} = E_{AB} - E_A - E_B \quad (9)$$

where E_{AB} represents the energy of the interacting super-system, and E_A and E_B represent the energies of the isolated systems.

3. Results and Discussion

Monomers **A**, **B**, and **C** were synthesized via Diels-Alder reaction of cyclopentadiene and the corresponding alkoxyvinylsilane derivative following standard procedures.^{41, 55} Each monomer was isolated as a clear liquid in moderate yield (30-60 %), and subsequently purified via successive vacuum distillations at reduced pressure until >99% purity was achieved, as determined via gas chromatography. Each monomer was characterized using ¹H NMR spectroscopy and high-resolution mass spectrometry (see Supporting Information). The *endo:exo* ratios for monomers **A**, **B**, and **C** were each determined using ¹H NMR spectroscopy and found to be 65:35, 62:38, and 38:62, respectively.

Monomers **A** and **B** were each homopolymerized using **Cat1** to yield poly(5-triethoxysilyl-2-norbornene) (**P1**) and poly(5-tris(2-methoxy-ethoxy)silyl-norbornene) (**P5**), respectively (Figure 3, top). Three random copolymers containing increasing ratios of monomers **A:B** were also synthesized (**P2-P4**) so that membrane performance could be tracked as a direct function of monomer incorporation ratio (**A:B**). To benchmark the gas separation performance of these polymers relative to other known membranes, we also synthesized the silane-containing VAPNB **P6**. Polymer **P6** has been extensively studied by Yampolskii *et al.* and is known to exhibit high permeability and modest selectivity for gases such as CO₂.⁵⁵ Monomer **C** was readily polymerized using **Cat2**, producing high molecular weight polymer **P6** that was cast into durable membranes for subsequent testing.⁵³⁻⁵⁴

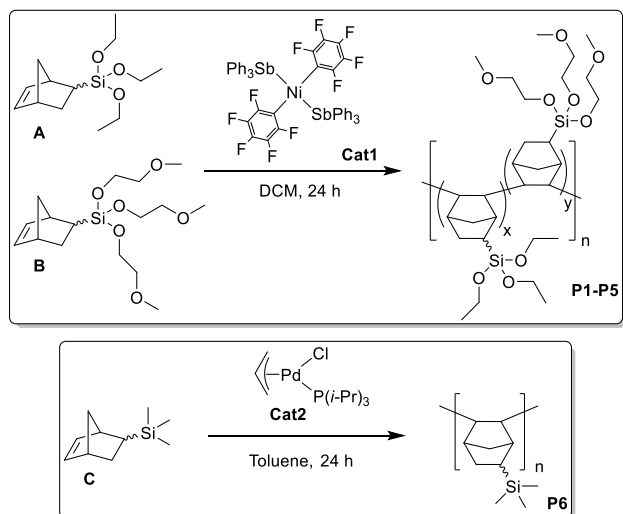


Figure 3. Synthesis of polymers **P1-P5** using **Cat1**, and synthesis of polymer **P6** using **Cat2**.

As shown in Table 1, the polymerization yield for **P1-P5** decreased as the molar ratio of **A:B** was decreased (71 → 44%); however, both molecular weight ($M_n = 115\text{--}176$ kg/mol) and dispersity ($D = 1.47\text{--}1.93$) remained relatively consistent (Table 1, entries 1-5). For copolymers **P2-P4**, ^1H NMR spectroscopy was used to confirm the incorporated monomer ratio (**A:B**) by comparing resonances at 3.86 and 1.32 ppm, which correspond to protons in the ethyl pendant groups of monomer **A**, to resonances at 4.00, 3.64, and 3.63 ppm, which correspond to the ethylene and terminal methoxy group of monomer **B**. In each case, the actual comonomer ratios favored higher incorporation of monomer **A** than was targeted in the feed (Table 1, entries 2-4). We hypothesize that this is due to a slower incorporation rate of monomer **B** due to its increased steric bulk, as compared to monomer **A**. Lastly, polymer **P6** was synthesized in 61% yield and achieved a molecular weight of 63 kg/mol (Table 1, entry 6).

Table 1. Polymerization and characterization of polymers **P1-P6**.^a

entry	polymer	feed	actual	yield	M_n^d	D^d
		ratio ^b	ratio ^c			
		(A:B)	(<i>x</i> : <i>y</i>)	(%)	(kg/mol)	
1	P1	100:0	100:0	71	143	1.47
2	P2	75:25	79:21	66	176	1.77
3	P3	50:50	59:41	54	175	1.64
4	P4	25:75	43:57	46	161	1.56

5	P5	0:100	0:100	44	115	1.93
6	P6	-	-	61	63	1.41

^aPolymerization conditions: total monomer concentration = 5 mmol, [Cat1] = 5 μ mol, 2 mL of DCM, T_{rxn} = 20 $^{\circ}$ C, and t = 24 h. ^bMolar ratio of monomers introduced into reaction. ^cActual monomer incorporation ratio (x:y) as described in Figure 3 and calculated via ¹H NMR spectroscopy.

^dMolecular weights and dispersity were measured using gel permeation chromatography at 40 $^{\circ}$ C in THF relative to polystyrene standards.

Alkoxysilyl-functionalized VAPNBs **P1-P5** and alkylsilyl-substituted VAPNB **P6** exhibit excellent solubility in many common organic solvents. Membranes of polymers **P1-P5** were solution cast from THF solutions to produce homogeneous films that typically ranged from 100-200 μ m in thickness. Membranes of polymer **P6** were cast from chloroform solutions, which was found to be an ideal casting solvent for this polymer. Dynamic mechanical analysis (DMA) revealed that polymers **P1-P5** are all high glass transition temperature, glassy polymers (T_g = 307–338 $^{\circ}$ C) (Table 2, entries 1-5), which is a typical trait of many previously reported VAPNBs, such as polymer **P6** that has a reported T_g of 373 $^{\circ}$ C (Table 2, entry 6).

Wide-angle x-ray scattering data for membranes **P1-P5** displayed only amorphous halos, confirming that these glassy materials have no crystallinity (see supporting information). Interchain spacing calculated from those measurements show that polymers **P1-P5** only vary by a few angstroms, indicating that their chain-packing remains relatively consistent across the polymer series. The density of polymers **P1-P5** were measured using Archimedes' Principle, and those values used to estimate their fractional free volume (FFV) using the Bondi Method (Table 2, entries 1-5). The density of polymers **P1-P5** generally increases as the mole fraction of incorporated monomer **B** is increased (density = 1.088 – 1.155); however, FFV estimation did not reveal any clear trends between monomer incorporation ratio (**A:B**) and free volume elements within these dense films. Perhaps most interestingly, the densities of alkoxysilane-substituted membranes **P1-P5** were consistently higher than trimethylsilyl-substituted **P6** (~1.1 versus 0.88 g/cm³) and their estimated FFV values were significantly lower (~0.165 versus 0.275) (Table 2, entries 1-6).

Table 2. Glass transition temperature, density, and fractional free volume (FFV) for films of polymers **P1-P6**.

entry	poly.	T_g^a ($^{\circ}$ C)	density (g/cm ³) ^b	FFV ^c
1	P1	338	1.088 (\pm 0.017)	0.159 (\pm 0.013)
2	P2	328	1.091 (\pm 0.003)	0.169 (\pm 0.003)
3	P3	323	1.111 (\pm 0.015)	0.164 (\pm 0.012)
4	P4	316	1.105 (\pm 0.014)	0.177 (\pm 0.010)
5	P5	307	1.155 (\pm 0.015)	0.158 (\pm 0.011)

6^d **P6** 373^d 0.883 (± 0.001)^d 0.275^d

^aMeasured using dynamic mechanical analysis. ^bDetermined using Archimedes' Principle. ^cEstimated using the Bondi Method. ^dData from literature.^{45, 55}

To test our hypothesis that adding more CO₂-philic functionalities to alkoxy-silane-substituted VAPNBs will enhance CO₂/N₂ separation performance, we measured ideal permeability and selectivity for membranes of **P1-P5** using the constant-volume variable-pressure gas flux method. As shown in Table 3, CO₂ permeability decreases from 936.6 to 754.8 Barrer (~19%) as the monomer incorporation ratio of **A:B** decreases along the series **P1** to **P5**, respectively (Table 3, entries 1 and 5). In contrast, N₂ permeability decreases much more substantially (57.3 to 20.7 Barrer), which represents a ~64% decrease in N₂ permeability as the mole fraction of incorporated monomer **B** is increased. The amalgamation of this minimal decrease in CO₂ permeability, but significant decrease in N₂ permeability, results in **P5** having a CO₂/N₂ selectivity of 36.7, which is approximately a 124% increase in selectivity as compared to polymer **P1**, which does not contain any monomers bearing ethylene glycol-like moieties.

Table 3. Ideal permeability and selectivity of polymers **P1-P6**.

entry	poly.	P (Barrer) ^a		α^b (CO ₂ /N ₂)
		CO ₂	N ₂	
1	P1	936.6 (± 14.9)	57.3 (± 2.3)	16.4 (± 0.4)
2	P2	868.8 (± 126)	40.5 (± 8.2)	21.6 (± 1.3)
3	P3	733.3 (± 66.7)	27.5 (± 4.2)	26.8 (± 1.6)
4	P4	700.0 (± 79.6)	19.6 (± 2.0)	33.7 (± 2.9)
5	P5	754.8 (± 40.5)	20.7 (± 2.6)	36.7 (± 2.8)
6	P6	4371 (± 855)	326.8 (± 7.7)	13.4 (± 2.4)

^aPermeability values of free-standing polymer films obtained using the constant-volume variable-pressure gas flux method at 30 psi upstream pressure.

^bIdeal selectivity calculated as P(CO₂)/P(N₂).

Comparing the ideal permeability and selectivity of alkoxy-silane-derived polymer **P5** to that of the previously reported trimethylsilyl-substituted **P6**, **P5** is an order of magnitude less permeable, but is ~174% more selective. This performance places membrane **P5** amongst the highest performing polymer membranes for the separation of CO₂ from N₂ and is perhaps best viewed visually in Figure 4, where the data for the polymer series **P1-P5** is plotted relative to the 2008 upper bound for CO₂/N₂ separation

performance. Furthermore, Figure 4 highlights that the polymer series **P1-P5** defies the traditional permeability-selectivity tradeoff, and moves vertically towards the upper bound rather than parallel to it as the polymer composition is systematically changed to contain more ethylene glycol-like units.⁸

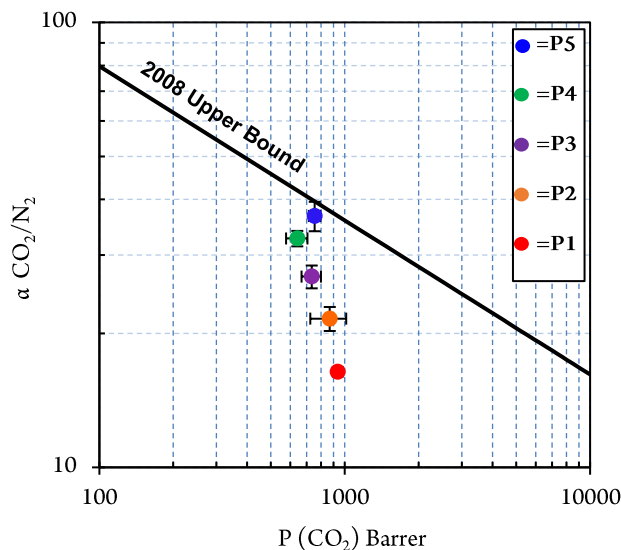


Figure 4. Robeson plot showing gas separation performance of polymers **P1-P5**. Error bars are included for each data point.

Encouraged by these results, we sought to further investigate the source of polymers **P1-P5**'s promising behavior. As described in Eq. 2, permeability (P) is the product of a membrane's concentration-averaged, effective diffusion coefficient (D) and solubility coefficient (S). To determine each of these coefficients, each membrane's pure gas solubility was measured using the dual-volume dual-transducer pressure decay method.⁵⁹ As can be seen in Figures 5-6, sorption isotherms were obtained for each polymer and that data was fit using either the dual-mode model or linearly, with all correlation factors (R^2) being ≥ 0.9997 for CO_2 and ≥ 0.9960 for N_2 . From those fits, pure gas solubility constants (S) were calculated as pressure approaches 0 atm. Finally, because P and S were both measured directly, D was then determined algebraically using the equation $D = P/S$.

From this data, we observed that alkoxy-silane-substituted polymers **P1-P5** all have similar diffusion coefficients for CO_2 , as well as for N_2 , and exhibit relatively small diffusivity selectivity values ($D(\text{CO}_2)/D(\text{N}_2) = 1.54 - 1.89$) (Table 4, entries 1-5). Therefore, this indicated that these membranes must primarily separate via solubility selectivity as their exceptional CO_2/N_2 selectivity cannot be explained via diffusivity values alone. Analysis of both CO_2 and N_2 solubility coefficient values indeed confirm this and reveal solubility selectivity values ranging from $S(\text{CO}_2)/S(\text{N}_2) = 10.1-19.3$ for polymers **P1-P5**, respectively (Table 4, entries 1-5). This increasing trend in solubility selectivity directly follows the increasing molar ratio of 5-tris(2-methoxyethoxy)silyl-2-norbornene units across this series of homo- and copolymers. Lastly, these results can be compared to silane-substituted polymer **P6**, which has a similar diffusivity selectivity ($D(\text{CO}_2)/D(\text{N}_2) = 1.92$), and significantly lower solubility selectivity ($S(\text{CO}_2)/S(\text{N}_2) = 6.97$) (Table 4, entry 6). We hypothesize that this is likely attributed to **P6**'s much higher fractional free volume (Table 2, entry 6), which can also be observed by its significantly higher diffusivity constants for both CO_2 and N_2 gases.

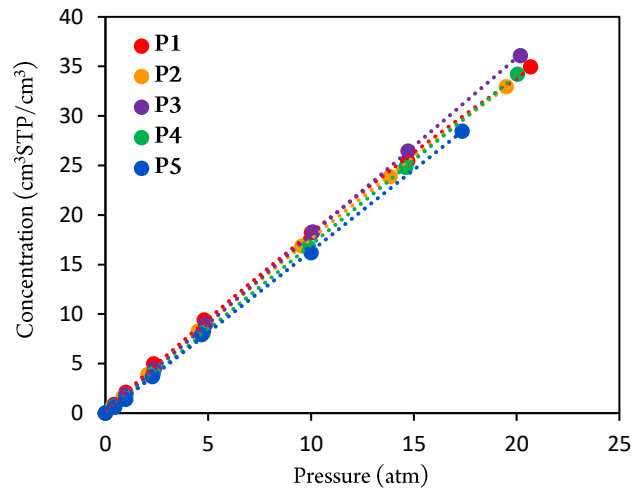


Figure 5. CO₂ sorption isotherms for polymers **P1-P5** at 35 °C. Polymers **P1-P3** were fit using the dual-mode model (Eq. 8), whereas polymers **P4-P5** were fit linearly to provide the highest possible correlation coefficient.

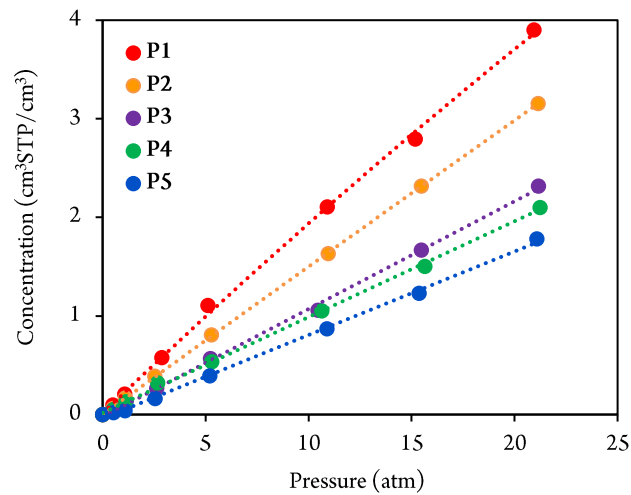


Figure 6. N₂ sorption isotherms for polymers **P1-P5** at 35 °C. Polymers **P1-P2** were fit using the dual-mode model (Eq. 8), whereas polymers **P3-P5** were fit linearly to provide the highest possible correlation coefficient.

Table 4. Diffusion coefficient, solubility coefficient, and Langmuir sorption parameters for polymers **P1-P6**.

entry	poly.	$D((\text{cm}^2/\text{s})\times 10^{-6})^{\text{a}}$			$S(\text{cm}^3\cdot[\text{STP}]/(\text{cm}^3\cdot\text{atm}))^{\text{b}}$			CO ₂			N ₂		
		$D(\text{CO}_2)/$		$D(\text{N}_2)$	$S(\text{CO}_2)/$		$S(\text{N}_2)$	k_{d}	C_{H}	b	k_{d}	C_{H}	b
		CO ₂	N ₂		CO ₂	N ₂							
1	P1	3.09	1.91	1.62	2.31	0.228	10.1	1.50	5.02	0.160	0.171	0.364	0.157
2	P2	3.38	2.01	1.68	1.95	0.154	12.7	1.54	4.79	0.086	0.148	0.032	0.172
3	P3	2.94	1.91	1.54	1.90	0.109	17.4	1.74	1.34	0.115	0.109	- ^c	- ^c
4	P4	3.12	1.85	1.69	1.71	0.097	17.6	1.71	- ^c	- ^c	0.097	- ^c	- ^c
5	P5	3.49	1.85	1.89	1.64	0.085	19.3	1.64	- ^c	- ^c	0.085	- ^c	- ^c
6	P6	4.93	2.57	1.92	6.73	0.966	6.97	1.82	45.5	0.108	0.572	4.75	0.083

^aDiffusion coefficients (D) were determined algebraically using the equation $D = P/S$. ^bSolubility coefficient (S) were measured using the dual-volume pressure decay method and reported as pressure approaches 0. ^cNot applicable as these isotherms were fit linearly.

Perhaps even more intriguing, though the solubility selectivity of polymers **P1-P5** increased as the concentration of CO₂-phillic ethylene glycol units were increased, all CO₂ solubility coefficients remained relatively constant ($S = 2.31\text{-}1.64 \text{ cm}^3\cdot[\text{STP}]/(\text{cm}^3\cdot\text{atm})$) (Table 4, entries 1-5). This observation directly argued against our initial hypothesis that by adding these presumably CO₂-philic ethylene glycol-based substituents (like found in **P5**), that their CO₂ solubility should be enhanced. In contrast, the data shows that the enhanced CO₂/N₂ selectivity of polymer **P5** ($S = 0.085 \text{ cm}^3\cdot[\text{STP}]/(\text{cm}^3\cdot\text{atm})$) arises primarily from its dramatically decreased N₂ solubility, relative to **P1** ($S = 0.228 \text{ cm}^3\cdot[\text{STP}]/(\text{cm}^3\cdot\text{atm})$).

Though elucidation of **P1-P5**'s individual diffusion and solubility coefficients provided essential insight, the fundamental intricacies of polymers **P1-P5**'s promising gas separation performance were still unclear. Unique features of these solubility selective polymers included their relatively similar CO₂ solubility coefficients and their dramatically decreasing N₂ solubility coefficients as the molar incorporation ratio of monomers containing ethylene glycol-like units was increased. Furthermore, polymers **P1-P5** each displayed either linear or nearly linear sorption isotherms (Figures 5-6, and Figures S3-S4 of the supporting information), which to the best of the author's knowledge has not been observed for other high T_g glassy polymers. To better understand this unique behavior, sorption isotherm fits were used to extract the Henry's Law dependent dissolution (k_{d}) and Langmuir contributions (where C_{H} is the Langmuir capacity parameter, and b is the Langmuir affinity parameter), to gas sorption as described by Eq. 8.

Analysis of these individual Henry's Law and Langmuir contributions to CO₂ sorption revealed several interesting trends for alkoxy-silane-substituted polymers **P1-P5**. The Henry's Law contributions remained relatively constant for polymers **P1-P5** ($k_a = 1.50-1.74$), and are similar to that obtained for polymer **P6** ($k_a = 1.82$) (Table 4). In contrast, Langmuir contributions to CO₂ sorption in polymers **P1-P3** exhibited a sharply decreasing trend in Langmuir capacity ($C_H = 5.02 \rightarrow 1.34$), whereas polymers **P4-P5** exhibited no Langmuir contribution at all, and were fit linearly to provide the highest possible correlation factor (R^2). This lack of Langmuir capacity is in stark contrast to polymer **P6**, which displays a Langmuir capacity of $C_H = 45.5$ (Table 4, entry 6), which is an order of magnitude higher than those observed for **P1-P3**. Because polymers **P1-P5**'s Langmuir contributions to sorption ($C_H \times b$) are virtually nonexistent, they display CO₂ sorption behavior that is primarily dominated by dissolution of CO₂ into the densified polymer matrix (Henry's Law dissolution) rather than into non-equilibrium excess free volume elements, which is atypical for glassy polymers. This also provides potential mechanistic rationale as to why **P1-P5**'s CO₂ sorption isotherms (Figure 5) and solubility coefficients are virtually constant.

In contrast to the relatively constant Henry's Law contributions (k_a) to CO₂ sorption observed for polymers **P1-P5**, a steadily decreasing trend in k_a was observed for N₂ solubility ($k_a = 0.171 \rightarrow 0.085$) (Table 4, entries 1-5). This decreasing trend directly corresponds to the increasing selectivity of polymers **P1-P5** and their increasing percentage of incorporated monomers containing ethylene glycol-like moieties (0 to 100%). Similarly, a decreasing trend in the N₂ Langmuir capacity of polymers **P1** and **P2** was also observed ($C_H = 0.364 \rightarrow 0.032$), while polymers **P3-P5** were fit linearly and no Langmuir components observed (Table 4, entries 1-5).

Upon considering the trends observed for both CO₂ and N₂ sorption, as well as their corresponding Henry's Law and Langmuir contributions, a few conclusions can be drawn. First, as the incorporated percentage of 5-tris(2-methoxyethoxy)-2-norbornene monomeric units in the polymer backbone is increased from 0 to 100% (**P1**→**P5**), a corresponding decrease in the Langmuir component ($C_H \times b$) is observed. This is evidenced by the exceedingly linear nature of their CO₂ and N₂ sorption isotherms (Figures 5-6), and as previously stated, is highly unusual for high T_g glassy polymers. Second, though the CO₂ solubility coefficients for polymers **P1-P5** were relatively similar, the sharp decrease in N₂ solubility coefficients is the dominant factor in the superior CO₂/N₂ pure gas selectivity of polymer **P5**. Further analysis revealed that the decreasing $S(N_2)$ values observed as 5-tris(2-methoxyethoxy)-2-norbornene monomer content is increased, can be attributed to the sharply decreasing solubility of N₂ within the densified matrix of the polymeric material (Henry's Law dissolution) and essentially nonexistent Langmuir contribution. This behavior is particularly intriguing and could be thought of as an N₂-phobic effect; however, explanations as to why such monomeric units might diminish the dissolution of a non-interacting, inert gas were unclear from our experimental investigations.

To better understand this unusual phenomenon, we performed electronic structure theory computations to aid in an explanation of polymer **P5**'s enhanced CO₂/N₂ selectivity in comparison to **P1**. Because experimental results showed that gas solubility within polymers **P1-P5** is primarily dominated by Henry's Law dissolution, both polymer-gas and polymer-polymer interactions are known to play key roles in gas diffusion.⁶⁹⁻⁷¹ To study these interactions, saturated monomers **A** and **B** were used as small molecule surrogates for polymers **P1** and **P5**, respectively, and monomer-gas and monomer-monomer interactions were computed.⁷²⁻⁷⁴

In regards to monomer-gas interactions, monomers **A** and **B** each contain silyl ether groups that interact favorably with CO₂ via both dispersion and induction forces. More specifically, the electron rich silyl ether oxygen atoms were shown to interact with the electron deficient carbon of CO₂, while the two oxygen atoms of CO₂ form weak hydrogen bonds with the adjacent hydrogen atoms within the monomers. The computed interaction energies for monomer **A**-CO₂ ($\Delta E_{1-\text{CO}_2}$) and monomer **B**-CO₂ ($\Delta E_{2-\text{CO}_2}$) are -4.1 and -6.1 kcal/mol, respectively, whereas the interaction energy for monomer **C** that lacks any silyl ether groups is about roughly half (-2.3 kcal/mol). The most stable conformation of the **B**-CO₂ super-system is shown in Figure 7 in which both the silyl ether and ethereal oxygen atoms were found to interact with CO₂, presumably leading to its more favorable $\Delta E_{2-\text{CO}_2}$ value. Monomers **A**, **B**, and **C** each showed only weak interactions with N₂ of -2.3, -1.9, and -1.6 kcal/mol, respectively.

To understand the relative stability of the gas interactions in the polymer, we needed to also calculate the monomer-monomer interaction energies (ΔE_{1-1} , ΔE_{5-5} and ΔE_{6-6}), which could then be compared to the monomer-gas energies. By comparing these values, we are able to provide insight into the relative energy barrier for perturbing the monomer-monomer intermolecular interactions by a particular gas. It is expected that a lower energy difference ($\Delta\Delta E$) between monomer-monomer and monomer-gas interactions correlates to easier Henry's Law dissolution of the gas molecule within the polymer matrix and therefore higher solubility values. The computed $\Delta\Delta E$ barriers are reported in Figure 8 in which monomer **C** has the lowest values of 4.6 kcal and 5.2 kcal/mol for CO₂ and N₂, respectively. This agrees well with experimental findings that show that **P6** has the greatest solubility for both gases, but because both the CO₂ and N₂ barriers are almost identical, **P6** provides the lowest solubility selectivity.

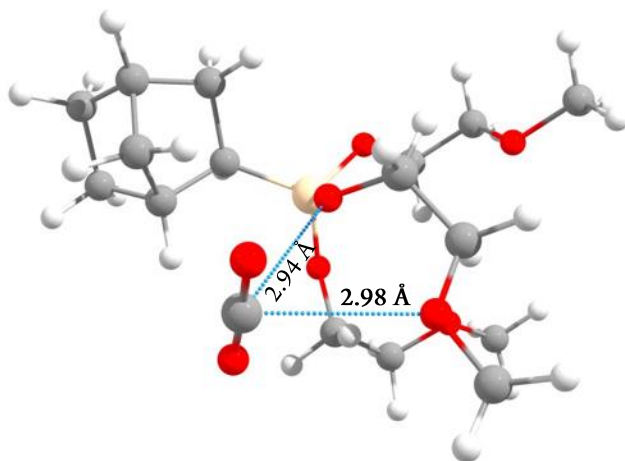


Figure 7. The most stable conformation for **B**-CO₂ contains favorable interactions between the two oxygen atoms of **B** and the electron-deficient carbon of CO₂. C_{CO2}-O₂ atom distances below 3.0 Å are shown.

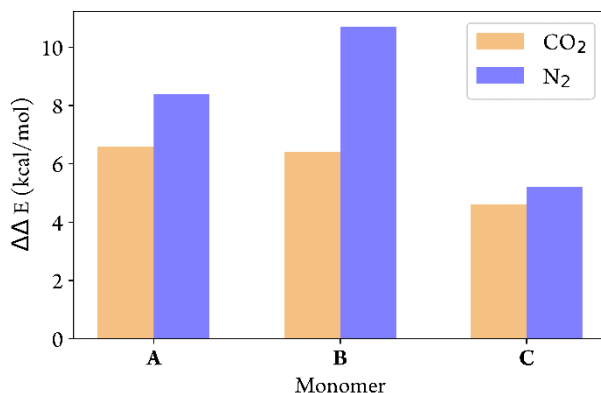


Figure 8. $\Delta\Delta E$ values for monomers **A**, **B**, and **C** with CO₂ and N₂.

The monomer-monomer interaction energies for two monomer **A**'s (ΔE_{1-1}) and two monomer **B**'s (ΔE_{2-2}) were calculated to be -10.7 and -12.6 kcal/mol, respectively. Though the interaction energy between two monomer **B**'s is clearly stronger, monomer **B** also interacts with CO₂ more strongly. As a result, both monomers **A** and **B** have very similar $\Delta\Delta E$ barriers for CO₂ of 6.6 and 6.4 kcal/mol, respectively, which agrees perfectly with the experimental observation that Henry's Law dissolution of CO₂ into both polymers **P5** and **P1** are essentially equal (Table 4, entries 1 and 5). In contrast, the $\Delta\Delta E$ values for monomers **A/B** and N₂ showed a more substantial difference of 8.4 and 10.7 kcal/mol, respectively. This result suggests that the Henry's Law dissolution of N₂ into polymer **P5** (signified by monomer **B**) is far more difficult than dissolution into polymer **P1** (signified by monomer **A**), and that **P5** should have a significantly decreased N₂ solubility coefficient relative to **P1**. These DFT results are in perfect agreement with their experimentally determined solubility coefficients for **P1** and **P5**, and therefore corroborate the greatly increased CO₂ selectivity observed for polymer **P5**, which occurs without a substantial loss in overall CO₂ permeability.

Having observed these exceptionally small or nonexistent degrees of Langmuir sorption in conjunction with slightly lower CO₂ sorption values, we collected mixed gas permeation data (Table 5) to complement our ideal gas permeation numbers. High pressure mixed gas permeation tests provide a more realistic perspective on membrane performance. For instance, membrane selectivities can suffer from deleterious CO₂ induced plasticization, which is increased by large degrees of CO₂ sorption. Furthermore, competitive sorption, whereby both gases compete for Langmuir sorption sites, can reduce CO₂ permeability due to the effective decrease in solubility. Considering the unique sorption behavior of VAPNBs **P1-P5**, the potential effects of plasticization and competitive sorption are particularly interesting.

Table 5. Mixed Gas Permeability and Selectivity of Polymers **P1-P5** at 800 psi and 25°C.^a

entry	polymer	P (Barrer) ^a		α^b (CO ₂ /N ₂)
		CO ₂	N ₂	
<hr/>				

1	P1	640.1(±15.1)	70.8(±0.5)	9.0(±0.1)
2	P2	523.9(±4.7)	45.3(±0.1)	11.6(±0.1)
3	P3	421.2(±6.7)	28.4(±0.1)	14.8(±0.3)
4	P4	400.1(±3.0)	21.3(±0.4)	18.8(±0.2)
5	P5	409.5(±12.7)	19.2(±0.1)	21.3(±0.5)

^aPermeability values of free-standing polymer films were obtained using the constant-volume variable-pressure gas flux method. ^bSelectivity calculated by a ratio of CO₂ and N₂ permeabilities.

In general, the mixed gas permeation results showed that CO₂ permeabilities and CO₂/N₂ selectivities are reduced under mixed gas feeds for polymers **P1-P5** (Table 5, Figure 9). Specifically, CO₂ permeabilities are reduced by 32-46% under 800 psi binary mixed gas conditions compared with pure gas values at 2 atm. This decrease in permeability could be consistent with the Langmuir contribution of the dual mode sorption model, which states that gas solubility is reduced as Langmuir sorption sites are filled at higher pressures;⁷⁵ however, pure gas sorption experiments demonstrated that several of these glassy polymers have little Langmuir sorption capacity (C_H). It follows that competitive sorption is not significant for **P4** and **P5** which exhibited entirely linear sorption isotherms for both CO₂ and N₂. These polymers behave more like rubbers in that sorption follows exclusively, or almost exclusively, Henry's Law. In this case, individual gas solubilities are independent of other components present.⁷⁵ However, mixed and pure gas permeabilities may also differ even in rubbery membranes. Yeom et. al. described a "coupling effect" that decreased solubility coefficients of PDMS when exposed to 15:85 binary mixture of CO₂:N₂ leading to decreased permeability coefficients.⁷⁶ Additional groups reported similar accounts of "negative coupling" in other rubbery polymer systems.⁷⁷ The exact mechanism for this behavior has not been detailed, but it demonstrates a possible rationale for the lower permeabilities exhibited by the VAPNBs presented in the current study in the absence of competitive sorption effects.

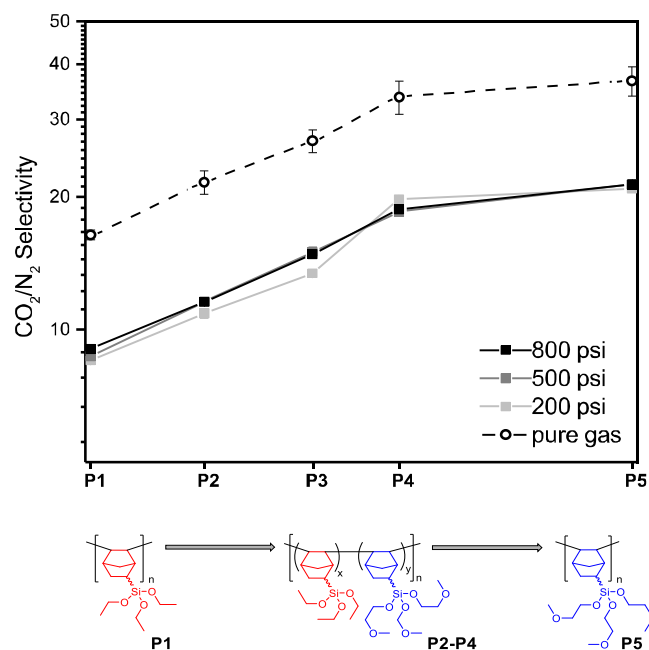


Figure 9. Pure and mixed gas selectivity plots as a function of increasing molar ratio of 5-tris(2-methoxyethoxy)-2-norbornene (shown in blue) content.

Plasticization in glassy polymers commonly leads to reduced selectivities and increased permeabilities. From Figure 9, it can be seen that the selectivity for each VAPNB remains unchanged as the feed pressure increases from 200 to 800 psi, signifying little to no plasticization. The extent of plasticization of glassy polymers is primarily dependent on the polymer chain rigidity (T_g) and activity of plasticizing species in the feed.⁷⁸ The VAPNBs **P1-P5** are unique glassy polymers, containing rigid backbones (and therefore high T_g) and low free volume which contribute to the observed plasticization resistance. While other examples of high T_g polymers with plasticization resistance exist, such as certain polyimides and polymers of intrinsic microporosity which have shown this resistance at CO_2 fugacities greater than 100 psi, it is still a somewhat uncommon trait in materials with high CO_2 uptake.⁷⁹⁻⁸² The Fox equation (Eq. 10) can be used to quantify the effect of diluents on the chain rigidity of membranes in mixed gas feeds, i.e. plasticization,⁷⁸

$$\frac{1}{T_{g,m}} = \frac{w_p}{T_{g,p}} + \frac{w_d}{T_{g,d}} \quad (10)$$

where w_p and w_d are the weight fractions of pure polymer and diluent respectively, and $T_{g,m}$, $T_{g,p}$, and $T_{g,d}$ are the glass transition temperatures of the polymer/diluent mixture, the pure polymer, and the CO_2 diluent (T_g of 108 K), respectively.⁷⁸ $T_{g,m}$ was calculated for **P1-P5** using pure gas solubility data from Table 4 and polymer densities and polymer T_g 's from Table 2. The values of $T_{g,m}$ ranged from 278 °C to 268 °C for **P1-P5** (values given in table S1). Given that the membranes are still well under their glass transition temperatures in the mixed gas feed, plasticization effects are negligible. The solubility of CO_2 in mixed gas may be lower due to the coupling effect, so the calculated $T_{g,m}$'s may be underestimating the true $T_{g,m}$'s. While the CO_2/N_2 selectivity drops 44% under high pressure mixed gas feeds compared to pure gas, plasticization is not the cause. Since plasticization and competitive sorption effects are not present in these polymer systems, it is hypothesized that the drop in selectivity under mixed gas conditions is due to the reduced solubility of CO_2 as a result of negative coupling.

Figure 10 represents the mixed gas data in terms of quantities relative to polymer **P1**. Despite the lower CO_2/N_2 selectivity observed in mixed gas compared to pure gas, the relative mixed gas selectivities follow a remarkably similar trend to the relative pure gas selectivity. As in pure gas, the mixed gas selectivity increases as 5-tris(2-methoxyethoxy)-2-norbornene content increases. Figure 10, bottom shows that both CO_2 and N_2 permeabilities decrease with increasing 5-tris(2-methoxyethoxy)-2-norbornene content, but the N_2 permeability decreases to a greater extent. This behavior was predicted in pure gas permeation tests as well as pure gas sorption experiments that showed the benefit in these ethylene glycol containing VAPNBs is their N_2 -phobicity. Pure gas relative solubility coefficients are also included to show that permeability decreases are directly related to losses in gas solubility within the polymers.

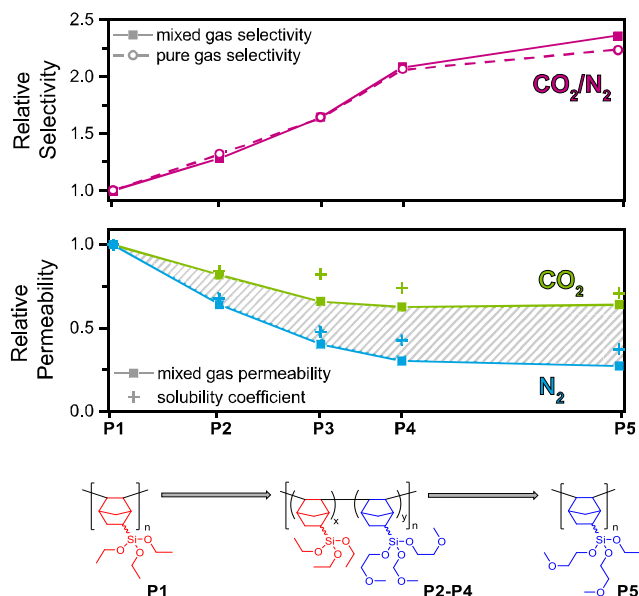


Figure 10. Relative selectivity (magenta) and permeability (green and blue) values of VAPNBs **P1-P5** relative to **P1** at 800 psi for mixed gas. Pure gas relative solubility coefficients (+) of **P1-P5** are overlaid with permeability data. The shaded area demonstrates the increase in CO₂/N₂ selectivity is brought about by exceedingly lower N₂ permeabilities relative to CO₂ permeabilities at high extents of 5-tris(2-methoxyethoxy)-2-norbornene content.

4. Conclusions

A series of VAPNBs (**P1-P5**) were designed and synthesized in which CO₂-philic, ethylene glycol-like units were systematically introduced via the monomer 5-tris(2-methoxyethoxy)-2-norbornene (**B**). Pure gas permeation testing revealed that as the molar ratio of **B:A** is increased, CO₂/N₂ selectivity is increased substantially with the highest performing membrane (**P5**) effectively reaching the 2008 Upper Bound ($P_{CO_2} = 754.8$ Barrer and $\alpha_{CO_2/N_2} = 36.7$). Though it was initially hypothesized that selectivity would be enhanced via increased CO₂ sorption, data clearly shows that the enhanced selectivity of **P5** results from its drastically decreased N₂ solubility. Such behavior has been referred to as N₂-phobicity in the literature.⁸³

Sorption isotherm analysis revealed that polymers **P1-P3** have minimal Langmuir contributions to CO₂ and N₂ sorption, whereas polymers **P4-P5** have no Langmuir contributions at all. To the best of the author's knowledge, the absence of any Langmuir contribution to sorption is remarkably rare for such high T_g , glassy polymers. To better understand the cause of this behavior and the enhanced selectivity of polymers **P2-P5**, computational chemistry was employed. These calculations suggest that the increased CO₂/N₂ selectivity of polymers **P2-P5** may result due to increased polymer-polymer and polymer-CO₂ associative interactions that arise from the incorporation of monomer **B**, but negligible increase in polymer-N₂ interactions.

Lastly, mixed gas permeation tests were performed to obtain permeability values closer to what could realistically be expected. In so doing, not only were such values obtained, but the capability of these alkoxy silane substituted membranes to separate mixed gas streams at high pressures (up to 800 psi) with minimal to no deleterious plasticization effects was observed. We attribute this behavior to the fact that our highest performing polymers (**P4-P5**) show no Langmuir contributions to sorption, seemingly sorbing

gases based purely on Henry's Law dissolution into their densified matrix, which as previously mentioned, has not yet been reported for high T_g glassy polymer membranes.

ASSOCIATED CONTENT

The Supporting Information is available free of charge on the ACS Publications Website at DOI: XXXX. Experimental details, monomer characterization, polymer GPCs, Cartesian coordinates from DFT.

AUTHOR INFORMATION

Corresponding Author

*Email: long@utk.edu

Acknowledgements

This work is supported by the U.S. Department of Energy, Office of Science, Office of Basic Energy Sciences, Chemical Sciences, Geosciences, and Biosciences Division, under Award Number DE-SC0018179. J. T. and K.D.V. would like to acknowledge the University of Tennessee for financial support of this work (start-up funds) and the Advanced Computer Facility (ACF) of the University of Tennessee for computational resources. S.M. performed X-ray diffraction measurements and contributed to data analysis and was supported by the U.S. Department of Energy (DOE), Office of Science, Basic Energy Sciences (BES), Chemical Sciences, Geosciences, and Biosciences Division. The authors would like to thank Huntsman Chemical for their generous donation of Matrimid 5218, and Prof. Benny Freeman for generously providing polycarbonate samples, which were each used to validate the permeation and sorption instruments used herein. The authors would also like to thank Prof. Benny Freeman and Melanie Merrick for their invaluable insight during the construction and validation of these instruments.

REFERENCES

- (1) see <https://www3.epa.gov/climatechange/science/>
- (2) Study, M. I., *The Future of Coal - Options for a Carbon Constrained World*. 2007.
- (3) see <https://www.epa.gov/ghgemissions/sources-greenhouse-gas-emissions>
- (4) Liu, J.; Hou, X.; Park, H. B.; Lin, H., High-Performance Polymers for Membrane CO₂ /N₂ Separation. *Chemistry* **2016**, *22* (45), 15980-15990.
- (5) see <https://www.epa.gov/cleanpowerplan/clean-power-plan-existing-power-plants>
- (6) Current and Future Technologies for Power Generation with Post-Combustion Carbon Capture (DOE/NETL-2012/1557), National Energy Technology Laboratory 2012

- (7) Merkel, T. C.; Lin, H.; Wei, X.; Baker, R., Power plant post-combustion carbon dioxide capture: An opportunity for membranes. *J. Membr. Sci.* **2010**, *359* (1-2), 126-139.
- (8) Robeson, L. M., The upper bound revisited. *J. Membr. Sci.* **2008**, *320* (1-2), 390-400.
- (9) Robeson, L. M., Correlation of Separation Factor Versus Permeability for Polymeric Membranes. *J. Membr. Sci.* **1991**, *62* (2), 165-185.
- (10) Robeson, L. M., Correlation of separation factor versus permeability for polymeric membranes. *J. Membr. Sci.* **1991**, *92*, 168-185.
- (11) Freeman, B. D., Basis of permeability/selectivity tradeoff relations in polymeric gas separation membranes. *Macromolecules* **1999**, *32* (2), 375-380.
- (12) Robeson, L. M.; Liu, Q.; Freeman, B. D.; Paul, D. R., Comparison of transport properties of rubbery and glassy polymers and the relevance to the upper bound relationship. *J. Membr. Sci.* **2015**, *476*, 421-431.
- (13) Robeson, L. M.; Smith, Z. P.; Freeman, B. D.; Paul, D. R., Contributions of diffusion and solubility selectivity to the upper bound analysis for glassy gas separation membranes. *J. Membr. Sci.* **2014**, *453*, 71-83.
- (14) Breck, D. W., *Zeolite Molecular Sieves: Structure, Chemistry, and Use*. John Wiley & Sons: New York, NY, 1974.
- (15) Mei Wu, X.; Gen Zhang, Q.; Ju Lin, P.; Qu, Y.; Mei Zhu, A.; Lin Liu, Q., Towards enhanced CO₂ selectivity of the PIM-1 membrane by blending with polyethylene glycol. *J. Membr. Sci.* **2015**, *493*, 147-155.
- (16) Tocci, E.; De Lorenzo, L.; Bernardo, P.; Clarizia, G.; Bazzarelli, F.; McKeown, N. B.; Carta, M.; Malpass-Evans, R.; Friess, K.; Pilnáček, K.; Lanč, M.; Yampolskii, Y. P.; Strarannikova, L.; Shantarovich, V.; Mauri, M.; Jansen, J. C., Molecular Modeling and Gas Permeation Properties of a Polymer of Intrinsic Microporosity Composed of Ethanoanthracene and Tröger's Base Units. *Macromolecules* **2014**, *47* (22), 7900-7916.
- (17) Carta, M.; Malpass-Evans, R.; Croad, M.; Rogan, Y.; Jansen, J. C.; Bernardo, P.; Bazzarelli, F.; McKeown, N. B., An Efficient Polymer Molecular Sieve for Membrane Gas Separations. *Science* **2013**, *339*, 303-307.
- (18) Du, N.; Park, H. B.; Robertson, G. P.; Dal-Cin, M. M.; Visser, T.; Scoles, L.; Guiver, M. D., Polymer nanosieve membranes for CO₂-capture applications. *Nat. Mater.* **2011**, *10* (5), 372-5.
- (19) Du, N.; Robertson, G. P.; Dal-Cin, M. M.; Scoles, L.; Guiver, M. D., Polymers of intrinsic microporosity (PIMs) substituted with methyl tetrazole. *Polymer* **2012**, *53* (20), 4367-4372.

- (20) Fritsch, D.; Bengtson, G.; Carta, M.; McKeown, N. B., Synthesis and Gas Permeation Properties of Spirobischromane-Based Polymers of Intrinsic Microporosity. *Macromol. Chem. Phys.* **2011**, *212* (11), 1137-1146.
- (21) Du, N.; Robertson, G. P.; Song, J.; Pinnau, I.; Thomas, S.; Guiver, M. D., Polymers of Intrinsic Microporosity Containing Trifluoromethyl and Phenylsulfone Groups as Materials for Membrane Gas Separation. *Macromolecules* **2008**, *41*, 9656-9662.
- (22) Budd, P.; McKeown, N.; Ghanem, B.; Msayib, K.; Fritsch, D.; Starannikova, L.; Belov, N.; Sanfirova, O.; Yampolskii, Y.; Shantarovich, V., Gas permeation parameters and other physicochemical properties of a polymer of intrinsic microporosity: Polybenzodioxane PIM-1. *J. Membr. Sci.* **2008**, *325* (2), 851-860.
- (23) Ghanem, B. S.; McKeown, N. B.; Budd, P. M.; Al-Harbi, N. M.; Fritsch, D.; Heinrich, K.; Starannikova, L.; Tokarev, A.; Yampolskii, Y., Synthesis, Characterization, and Gas Permeation Properties of a Novel Group of Polymers with Intrinsic Microporosity: PIM-Polyimides. *Macromolecules* **2009**, *42* (20), 7881-7888.
- (24) Mizumoto, T.; Masuda, T.; Higashimura, T., Polymerization of [o-(Trimethylgermyl)phenyl]acetylene and Polymer Characterization. *J. Polym. Sci., Part A: Polym. Chem.* **1993**, *31*, 2555-2561.
- (25) Morisato, A.; Shen, H. C.; Sankar, S. S.; Freeman, B. D.; Pinnau, I.; Casillas, C. G., Polymer characterization and gas permeability of poly(1-trimethylsilyl-1-propyne) [PTMSP], poly(1-phenyl-1-propyne) [PPP], and PTMSP/PPP blends. *J. Polym. Sci. B.* **1996**, *34* (13), 2209-2222.
- (26) Merkel, T. C.; Gupta, R. P.; Turk, B. S.; Freeman, B. D., Mixed-gas permeation of syngas components in poly(dimethylsiloxane) and poly(1-trimethylsilyl-1-propyne) at elevated temperatures. *J. Membr. Sci.* **2001**, *191*, 85-94.
- (27) Nagai, K.; Masuda, T.; Nakagawa, T.; Freeman, B. D.; Pinnau, I., Poly[1-(trimethylsilyl)-1-propyne] and related polymers: synthesis, properties and functions. *Prog. Polym. Sci.* **2001**, *26* (5), 721-798.
- (28) Gomes, D.; Nunes, S. P.; Peinemann, K.-V., Membranes for gas separation based on poly(1-trimethylsilyl-1-propyne)-silica nanocomposites. *J. Membr. Sci.* **2005**, *246* (1), 13-25.
- (29) Hong, T.; Zhenbin, N.; Xunxiang, H.; Gmernicki, K.; Cheng, S.; Fan, F.; Johnson, C.; Hong, E.; Mahurin, S. M.; Jiang, D.-e.; Long, B.; Mays, J.; Sokolov, A.; Saito, T., Effect of Cross-Link Density on Carbon Dioxide Separation in Polydimethylsiloxane-Norbornene Membranes. *ChemSusChem* **2015**, *8* (21), 3524.

- (30) Senthilkumar, U.; Reddy, B., Polysiloxanes with pendent bulky groups having amino-hydroxy functionality: Structure–permeability correlation. *J. Membr. Sci.* **2007**, *292* (1-2), 72-79.
- (31) Lin, H.; Freeman, B. D., Gas solubility, diffusivity and permeability in poly(ethylene oxide). *J. Membr. Sci.* **2004**, *239* (1), 105-117.
- (32) Wang, Y.; Li, H.; Dong, G.; Scholes, C.; Chen, V., Effect of Fabrication and Operation Conditions on CO₂ Separation Performance of PEO–PA Block Copolymer Membranes. *Ind. Eng. Chem. Res.* **2015**, *54* (29), 7273-7283.
- (33) Wang, Y. Y.; Hu, T.; Li, H. Y.; Dong, G. X.; Wong, W.; Chen, V., Enhancing membrane permeability for CO₂ capture through blending commodity polymers with selected PEO and PEO-PDMS copolymers and composite hollow fibres. *12th International Conference on Greenhouse Gas Control Technologies, Ghgt-12* **2014**, *63*, 202-209.
- (34) Tena, A.; Marcos-Fernández, A.; Lozano, A. E.; de Abajo, J.; Palacio, L.; Prádanos, P.; Hernández, A., Influence of the PEO length in gas separation properties of segregating aromatic–aliphatic copoly(ether-imide)s. *Chem. Eng. Sci.* **2013**, *104*, 574-585.
- (35) Liu, S. L.; Shao, L.; Chua, M. L.; Lau, C. H.; Wang, H.; Quan, S., Recent progress in the design of advanced PEO-containing membranes for CO₂ removal. *Prog. Polym. Sci.* **2013**, *38* (7), 1089-1120.
- (36) Yampolskii, Y.; Starannikova, L.; Belov, N.; Bermeshev, M.; Gringolts, M.; Finkelshtein, E., Solubility controlled permeation of hydrocarbons: New membrane materials and results. *J. Membr. Sci.* **2014**, *453*, 532-545.
- (37) Finkelshtein, E. S.; Bermeshev, M. V.; Gringolts, M. L.; Starannikova, L. E.; Yampolskii, Y. P., Substituted polynorbornenes as promising materials for gas separation membranes. *Russ. Chem. Rev.* **2011**, *80* (4), 341-361.
- (38) Bermeshev, M. V.; Syromolotov, A. V.; Gringolts, M. L.; Starannikova, L. E.; Yampolskii, Y. P.; Finkelshtein, E. S., Synthesis of High Molecular Weight Poly[3-{tris(trimethylsiloxy)silyl}tricyclononenes-7] and Their Gas Permeation Properties. *Macromolecules* **2011**, *44* (17), 6637-6640.
- (39) Starannikova, L.; Pilipenko, M.; Belov, N.; Yampolskii, Y.; Gringolts, M.; Finkelshtein, E., Addition-type polynorbornene with Si(CH₃)₃ side groups: Detailed study of gas permeation and thermodynamic properties. *J. Membr. Sci.* **2008**, *323* (1), 134-143.

- (40) Finkelshtein, E. S.; Makovetskii, K. L.; Gringolts, M. L.; Rogan, Y. V.; Golenko, T. G.; Starannikova, L. E.; Yampolskii, Y. P.; Shantarovich, V. P.; Suzuki, T., Addition-Type Polynorbornenes with Si(CH₃)₃ Side Groups: Synthesis, Gas Permeability, and Free Volume. *Macromolecules* **2006**, *39*, 7022-7029.
- (41) Gmernicki, K. R.; Hong, E.; Maroon, C. R.; Mahurin, S. M.; Sokolov, A. P.; Saito, T.; Long, B. K., Accessing Siloxane Functionalized Polynorbornenes via Vinyl-Addition Polymerization for CO₂ Separation Membranes. *ACS Macro Lett.* **2016**, *5* (7), 879-883.
- (42) Koros, W. J., Simplified Analysis of Gas, Polymer Selective Solubility Behavior. *J. Poly. Sci. B: Poly. Phys.* **1985**, *23*, 1611-1628.
- (43) Lin, H. Q.; Freeman, B. D., Materials selection guidelines for membranes that remove CO₂ from gas mixtures. *J. Mol. Struct.* **2005**, *739* (1-3), 57-74.
- (44) Kazarian, S. G.; Vincent, M. F.; Bright, F. V.; Liotta, C. L.; Eckert, C. A., Specific Intermolecular Interaction of Carbon Dioxide with Polymers. *J. Am. Chem. Soc.* **1996**, *118*, 1729-1736.
- (45) Sundell, B. J.; Lawrence, J. A.; Harrigan, D. J.; Vaughn, J. T.; Pilyugina, T. S.; Smith, D. R., Alkoxysilyl functionalized polynorbornenes with enhanced selectivity for heavy hydrocarbon separations. *RSC Adv.* **2016**, *6* (57), 51619-51628.
- (46) Belov, N.; Nikiforov, R.; Starannikova, L.; Gmernicki, K. R.; Maroon, C. R.; Long, B. K.; Shantarovich, V.; Yampolskii, Y., A detailed investigation into the gas permeation properties of addition-type poly(5-triethoxysilyl-2-norbornene). *Eur. Polym. J.* **2017**, *93*, 602-611.
- (47) Vaughn, J. T.; Harrigan, D. J.; Sundell, B. J.; Lawrence, J. A.; Yang, J., Reverse selective glassy polymers for C₃+ hydrocarbon recovery from natural gas. *J. Membr. Sci.* **2017**, *522*, 68-76.
- (48) Tian, Z.; Saito, T.; Jiang, D. E., Ab Initio Screening of CO₂-philic Groups. *J. Phys. Chem. A* **2015**, *119* (16), 3848-52.
- (49) Vogiatzis, K. D.; Klopper, W.; Friedrich, J., Non-covalent Interactions of CO₂ with Functional Groups of Metal-Organic Frameworks from a CCSD(T) Scheme Applicable to Large Systems. *J. Chem. Theory Comput.* **2015**, *11* (4), 1574-84.
- (50) Yave, W.; Car, A.; Funari, S. S.; Nunes, S. P.; Peinemann, K. V., CO₂-Philic Polymer Membrane with Extremely High Separation Performance. *Macromolecules* **2010**, *43* (1), 326-333.

- (51) Okamoto, K.-i.; Fujii, M.; Okamoto, S.; Suzuki, H.; Tanaka, K.; Kita, H., Gas Permeation of Properties of Poly(ether imide) Segmented Copolymers. *Macromolecules* **1995**, *28*, 6950-6956.
- (52) Casares, J. A.; Espinet, P.; Martin-Alvarez, J. M.; Martinez-Ilarduya, J. M.; Salas, G., Stable nickel catalysts for fast norbornene polymerization: Tuning reactivity. *Eur. J. Inorg. Chem.* **2005**, *2005* (19), 3825-3831.
- (53) Kim, D.-G.; Bell, A.; Register, R. A., Living Vinyl Addition Polymerization of Substituted Norbornenes by a t-Bu₃P-Ligated Methylpalladium Complex. *ACS Macro Lett.* **2015**, *4* (3), 327-330.
- (54) Kim, D. G.; Takigawa, T.; Kashino, T.; Burtovyy, O.; Bell, A.; Register, R. A., Hydroxyhexafluoroisopropylnorbornene Block and Random Copolymers via Vinyl Addition Polymerization and Their Application as Biobutanol Pervaporation Membranes. *Chem. Mater.* **2015**, *27* (19), 6791-6801.
- (55) Finkelshtein, E. S.; Makovetskii, K. L.; Gringolts, M. L.; Rogan, Y. V.; Golenko, T. G.; Starannikova, L. E.; Yampolskii, Y. P.; Shantarovich, V. P.; Suzuki, T., Addition-type polynorbornenes with Si(CH₃)₃ side groups: Synthesis, gas permeability, and free volume. *Macromolecules* **2006**, *39* (20), 7022-7029.
- (56) Jagodzinski, H., H. P. Klug und L. E. Alexander: X-ray Diffraction Procedures for Polycrystalline and Amorphous Materials, John Wiley & Sons, New York-Sydney-Toronto 1974. *Berichte der Bunsengesellschaft für physikalische Chemie* **1975**, *79* (6), 553-553.
- (57) McHattie, J. S.; Koros, W. J.; Paul, D. R., Gas transport properties of polysulphones: 1. Role of symmetry of methyl group placement on bisphenol rings. *Polymer* **1991**, *32* (5), 840-850.
- (58) Czichos, H.; Saito, T.; Smith, L., *Springer Handbook of Materials Measurement Methods*. 2006.
- (59) Koros, W. J.; Paul, D. R., Design Considerations for Measurement of Gas Sorption in Polymers by Pressure Decay. *J. Polym. Sci. B.* **1976**, *14* (10), 1903-1907.
- (60) Bevington, P. R., *Data Reduction and Error Analysis for the Physical Sciences*. McGraw-Hill: New York, 1969.
- (61) Jorgensen, W. L.; Maxwell, D. S.; TiradoRives, J., Development and testing of the OPLS all-atom force field on conformational energetics and properties of organic liquids. *J. Am. Chem. Soc.* **1996**, *118* (45), 11225-11236.
- (62) Dodda, L. S.; Cabeza de Vaca, I.; Tirado-Rives, J.; Jorgensen, W. L., LigParGen web server: an automatic OPLS-AA parameter generator for organic ligands. *Nucleic Acids Res.* **2017**, *45* (W1), W331-W336.

- (63) Plimpton, S., Fast Parallel Algorithms for Short-Range Molecular-Dynamics. *J. Comput. Phys.* **1995**, *117* (1), 1-19.
- (64) Ahlrichs, R.; Bar, M.; Haser, M.; Horn, H.; Kolmel, C., Electronic-Structure Calculations on Workstation Computers - the Program System Turbomole. *Chem. Phys. Lett.* **1989**, *162* (3), 165-169.
- (65) Adamo, C.; Barone, V., Toward reliable density functional methods without adjustable parameters: The PBE0 model. *J. Chem. Phys.* **1999**, *110* (13), 6158-6170.
- (66) Weigend, F., Hartree-Fock exchange fitting basis sets for H to Rn. *J. Comput. Chem.* **2008**, *29* (2), 167-75.
- (67) Grimme, S.; Antony, J.; Ehrlich, S.; Krieg, H., A consistent and accurate ab initio parametrization of density functional dispersion correction (DFT-D) for the 94 elements H-Pu. *J. Chem. Phys.* **2010**, *132* (15), 154104.
- (68) Grimme, S.; Ehrlich, S.; Goerigk, L., Effect of the damping function in dispersion corrected density functional theory. *J. Comput. Chem.* **2011**, *32* (7), 1456-65.
- (69) Barbari, T. A.; Koros, W. J.; Paul, D. R., Gas Sorption in Polymers Based on Bisphenol-A. *J. Polym. Sci. B.* **1988**, *26* (4), 729-744.
- (70) Sefcik, D. R. a. M. D., Gas Transport and Cooperative Main-Chain Motions in Glassy Polymers. In *Industrial Gas Separations*, American Chemical Society: Washington, DC, 1983.
- (71) Sefcik, D. R. a. M. D., Sorption and Transport in Glassy Polymers. American Chemical Society: Washington, DC., 1983.
- (72) Kilic, S.; Wang, Y.; Johnson, J. K.; Beckman, E. J.; Enick, R. M., Influence of tert-amine groups on the solubility of polymers in CO₂. *Polymer* **2009**, *50* (11), 2436-2444.
- (73) Feng, H. B.; Hong, T.; Mahurin, S. M.; Vogiatzis, K. D.; Gmernicki, K. R.; Long, B. K.; Mays, J. W.; Sokolov, A. P.; Kang, N. G.; Saito, T., Gas separation mechanism of CO₂ selective amidoxime-poly(1-trimethylsilyl-1-propyne) membranes. *Polym. Chem.* **2017**, *8* (21), 3341-3350.
- (74) Zulfikar, S.; Karadas, F.; Park, J.; Deniz, E.; Stucky, G. D.; Jung, Y.; Atilhan, M.; Yavuz, C. T., Amidoximes: promising candidates for CO₂ capture. *Energy Environ. Sci.* **2011**, *4* (11), 4528-4531.
- (75) Koros, W. J., Model for sorption of mixed gases in glassy polymers. *J. Poly. Sci.: Poly. Phys. Ed.* **1980**, *18* (5), 981-992.

- (76) Yeom, C. K.; Lee, S. H.; Lee, J. M., Study of transport of pure and mixed CO₂/N₂ gases through polymeric membranes. *J. Appl. Poly. Sci.* **2000**, 78 (1), 179-189.
- (77) Reijerkerk, S. R.; Knoef, M. H.; Nijmeijer, K.; Wessling, M., Poly(ethylene glycol) and poly(dimethyl siloxane): Combining their advantages into efficient CO₂ gas separation membranes. *J. Membr. Sci.* **2010**, 352 (1-2), 126-135.
- (78) Lin, H.; Yavari, M., Upper bound of polymeric membranes for mixed-gas CO₂/CH₄ separations. *J. Membr. Sci.* **2015**, 475, 101-109.
- (79) Swaidan, R.; Ghanem, B.; Litwiller, E.; Pinnau, I., Physical Aging, Plasticization and Their Effects on Gas Permeation in “Rigid” Polymers of Intrinsic Microporosity. *Macromolecules* **2015**.
- (80) Yong, W. F.; Chung, T.-S., Miscible blends of carboxylated polymers of intrinsic microporosity (cPIM-1) and Matrimid. *Polymer* **2015**, 59 (0), 290-297.
- (81) Alaslai, N.; Ghanem, B.; Alghunaimi, F.; Pinnau, I., High-performance intrinsically microporous dihydroxyl-functionalized triptycene-based polyimide for natural gas separation. *Polymer* **2016**, 91, 128-135.
- (82) Wind, J. D.; Paul, D. R.; Koros, W. J., Natural gas permeation in polyimide membranes. *J. Membr. Sci.* **2004**, 228 (Copyright (C) 2014 American Chemical Society (ACS). All Rights Reserved.), 227-236.
- (83) Patel, H. A.; Je, S. H.; Park, J.; Chen, D. P.; Jung, Y.; Yavuz, C. T.; Coskun, A., Unprecedented high-temperature CO₂ selectivity in N₂-phobic nanoporous covalent organic polymers. *Nat. Commun.* **2013**, 4, 1357.

Insert Table of Contents artwork here

